RSC Advances

ROYAL SOCIETY OF CHEMISTRY

www.rsc.org/advances

Journal Name

RSCPublishing

ARTICLE

Macroporous network $Li_3V_2(PO_4)_3$/C cathode material with excellent high-rate performance for lithium-ion battery

Cite this: DOI: 10.1039/xoxxoooooox

Received ooth January 2012,
Accepted ooth January 2012

DOI: 10.1039/xoxxoooooox

www.rsc.org/

Xiu-Shan Yang,[a] Yan-Ying Wang,[a] Yan-Jun Zhong,[a] Ben-He Zhong,[a] Yan Tang*[a, b]

Macroporous network $Li_3V_2(PO_4)_3$/C was successfully synthesized by rheological phase method using ethanol and 1,2-propylene glycol as a mixed solvent. At the same time, the $Li_3V_2(PO_4)_3$/C via a single ethanol solvent was prepared for comparison. XRD analysis of the two samples confirmed the formation of high purity and well-crystallized $Li_3V_2(PO_4)_3$/C. The SEM results reveal that there is a significant difference in morphologies between the two samples, the one by single ethanol shows a flake-like morphology, while the other one presents macroporous network morphology. The sample with a macroporous network morphology shows discharge capacities of 154, 138, 130, 120, 101, 93, 83 and 70 mAh g^{-1} at 1 C, 3 C, 5 C, 10 C, 20 C, 30 C, 40 C and 50 C (1C=150 mA g^{-1}) in the voltage range of 3.0-4.8 V, respectively, which are better than those of $Li_3V_2(PO_4)_3$/C sample with a flake-like morphology. In summary, it is demonstrated that the $Li_3V_2(PO_4)_3$/C cathode material using mixed solvent can deliver a significantly improved high rate performance in the voltage range of 3.0-4.8 V, which can be mainly ascribed to the macroporous network morphology.

1. Introduction

Nowadays, in order to meet the needs of energy crisis and emerging environment concerns, lithium ion batteries with excellent electrochemical performance and environmentally friendly features have been getting increasing intense attention. [1] Among lithium transition metal phosphates such as $LiMPO_4$ (M = Fe, Co, Mn) and $Li_3M_2(PO_4)_3$ (M = V, Fe), monoclinic $Li_3V_2(PO_4)_3$(LVP) has attracted intensive attention, due to its superior thermal stability, large theoretic specific capacity, environmental benign and abundant resource and so on.[2,3] It can obtain a theoretical capacity of 133 mAh g^{-1} with two lithium ions reversibly delivering in the potential range of 3.0-4.3 V. When the third lithium ions are completely extracted in the wider voltage window (3.0-4.8 V), the specific capacity of LVP reach up to 197 mAh g^{-1} but fades rapidly as a result of structural instability.[4]

Besides, its inherent poor electronic conductivity and lithium ion diffusion coefficient lead to a poor rate capability and discharge capacity. Multiple strategies are reported to improve the rate performance of LVP, such as carbon coating,[5,6] oxide modification,[7-9] cation doping,[10,11] nanotechnologies[12,13] and controlling morphologies of particles.[14,15] Our group have done a lot of work about morphology control aiming to improve the electrochemical performance of $Li_3V_2(PO_4)_3$/C.[16-18] A flake-like $Li_3V_2(PO_4)_3$/C was successfully synthesized by rheological phase method using PVA as template in our previous work,[16] and it exhibits excellent high-rate performance in voltage range of 3.0-4.5 V. Porous $Li_3V_2(PO_4)_3$/C material synthesized by sol-gel combustion method with NH_4NO_3 as additive also display considerable electrochemical performances.[17]

In this paper, the strategies of flake-like and porous structure are combined together by a novel rheological phase method using ethanol and 1,2-propylene glycol as a mixed solvent, and $Li_3V_2(PO_4)_3$/C (LVP/C-B) with an open macroporous network morphology is resulted. For comparison, another LVP/C-A sample is also prepared via the same method using single ethanol. The morphologies and electrochemical performances of the two samples are detailed investigated.

2. Experimental section

2.1 Sample preparation

$Li_3V_2(PO_4)_3$/C composite was prepared via a novel rheological phase method using LiH_2PO_4, V_2O_5, stearic acid and polyvinyl alcohol (PVA-1799) as the raw materials. All the raw materials were analytically pure grade and provided by Chengdu Kelong Chemical Co., China. Stearic acid was used as carbon source and PVA was employed as template reagent. Firstly, a mixture of ethanol and 1,2-propylene glycol in proportion of 20:1 (volume ratio) as the mixed solvent has been prepared. Secondly, 0.3 mole LiH_2PO_4 and 0.1 mole V_2O_5, 3g stearic acid and 0.5g PVA were dispersed in proper mixed solvent by ball milling for 2 hours in a high speed vibrating ball miller (SFM-3, 1200 rpm, MTI Co.). The obtained pasty precursor was dried at 90 °C for 6 hours in an air dry oven to evaporate solvent. Finally, the dried precursor was reground and calcined at 700 °C for 4 hours in a tube furnace under Ar atmosphere to obtain the $Li_3V_2(PO_4)_3$/C composite (labeled as LVP/C-B). For comparison, $Li_3V_2(PO_4)_3$/C composite (labeled as LVP/C-A) using the single ethanol solvent was also prepared by the identical process.

2.2 Sample characterization

TG-DTA analysis of the precursor was performed by TG-209F1 (Netzsch, Germany) device during the temperature ranging from 30 °C to 1000 °C at the heating rate of 10 °C min^{-1} under a N_2 flow of 20 ml min^{-1}. The crystalline structure of each product was recorded by X-ray diffraction (XRD, D/max-rB, Rigaku, by using Cu Kα radiation with the λ=0.15046 nm). The residual carbon content of the materials was tested by CS-902 (Wanlianda Xinke Co., China) analytical device. The microscopic morphologies of $Li_3V_2(PO_4)_3$/C particles were observed by scanning electron microscopy (SEM, HITACHI S-4800). The specific surface areas and the pore size distributions were evaluated by a computer-controlled sorption analyzer (QuadraSorb SI, Quantachrome). The composition and valence state of V at the surface and 10 nm deep etching of $Li_3V_2(PO_4)_3$/C were tested by X-ray photoelectron spectroscopy (XPS, Quantum 2000, Physical Electronics corporation).

2.3 Electrochemical measurement

The cathode electrode was fabricated by mixing the obtained active powder, acetylene black and polyvinylidene fluoride (PVDF) in a weight ratio of 80:13:7 in N-methyl-2-pyrrolidinone (NMP). The resultant slurry was spread uniformly onto a smooth aluminum foil and dried at 100 °C for 15 h in vacuum and then cut into slices with an area of 1.54 cm^2. The average and standard deviation of the mass loadings of the cathodesare 2.25 mg and 0.43 mg.The lithium metal foil was used as counter electrode, Celgard 2400 as the separator, and 1 mol L^{-1} $LiPF_6$ dissolved in the mixture of ethylene carbonate and dimethyl carbonate (EC/DMC, 1:1 by volume) as electrolyte. The CR2032 cells were assembled in a glove box filled with high-purity argon. The cells were cycled at different C-rates between 3.0 and 4.8 V on a cell testing instrument (NEWARE, China). The electrochemical impedance spectra (EIS) measurements were performed on a Zennium electrochemical work station (Zahner), and EIS spectra were recorded over a frequency range from 100 kHz to 10 mHz with an AC amplitude of 5 mV.

3. Results and discussion

Fig.1 shows the TG-DTA curves of LVP/C-B precursor from 30 °C to 1000 °C. About 31.46% weight-loss of the precursor is observed from 30 °C to 700 °C. The weight loss can be roughly divided into three parts, namely 30-150 °C, 150-400 °C, and 400-700 °C. The weight loss in the first region (i.e. 30-150 °C) is ascribed to the release and evaporation of the adsorbed water. In the second region (i.e. 150-400 °C), there is an endothermic peak can be seen obviously from the c-DTA curve, which is due to the pyrolysis of stearic acid, PVA and 1,2-propylene glycol, and accordingly induced large weight loss in the TG curves. A relatively small weight loss in the temperature range of 400-700 °C can be ascribed to the formation of LVP/C product, accompanied by exothermic peak in the c-DTA curve. Above 700 °C, there is no evident mass loss in the TG curve, which indicates the completion of the entire reaction. In the calcination process, a lot of gas generated from the pyrolysis of carbon sources causes the pore structure of the product. And the residual carbon is evenly coated on the surface of the particles.

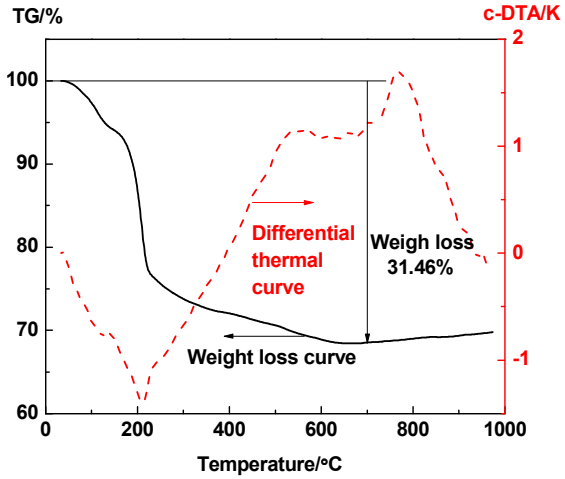

Fig.1 TG and c-DTA curves of the LVP/C-B precursor recorded at the heating rate of 10 °C min^{-1} under a N_2 flow of 20 ml min^{-1}

Fig.2 shows the X-ray diffraction (XRD) patterns of LVP/C-A and LVP/C-B. The sharp diffraction peaks indicate that the two samples are well-crystallized, and can be assigned to monoclinic $Li_3V_2(PO_4)_3$ with the space group of $P2_1/n$ (PDF#01-072-7074), which are in good agreement with the previous reports.[19-21] Element analysis of the final products reveal that the carbon contents of LVP/C-A and LVP/C-B are 3.14% and 3.22%, respectively. There is no evidence of diffraction patterns corresponding to carbon, indicating that the residual carbon is in an amorphous structure.

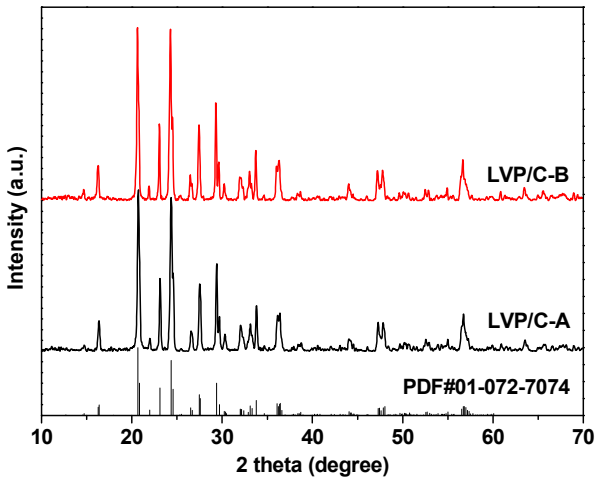

Fig.2 XRD patterns for the as-prepared LVP/C-A and LVP/C-B.

Fig.3 shows the XPS spectra of LVP/C-B at the surface and in the interior (10 nm deep etching). The oxidation states of the elements in $Li_3V_2(PO_4)_3$/C can be observed and no other impurity elements could be indexed on the peak. From Fig. 3(b), it can be seen that the intensity of C1s is stronger in the surface than that in the interior, indicating that the carbon mainly exist at the surface of the sample. From Fig. 3c, obviously difference of the V2p oxidation states can be observed in the surface and in the interior. From Fig. 3(d-e), the observed binding energies at 515.9eV and 517.1eV are consistent with the previous report for V^{3+} (V_2O_3) and V^{5+} (V_2O_5). The contents of V^{3+} at the surface and in the interior are 16% and 41% calculated by the areas of the peaks, indicating that the V^{3+} is easy oxidized in air.

Journal Name

RSCPublishing

ARTICLE

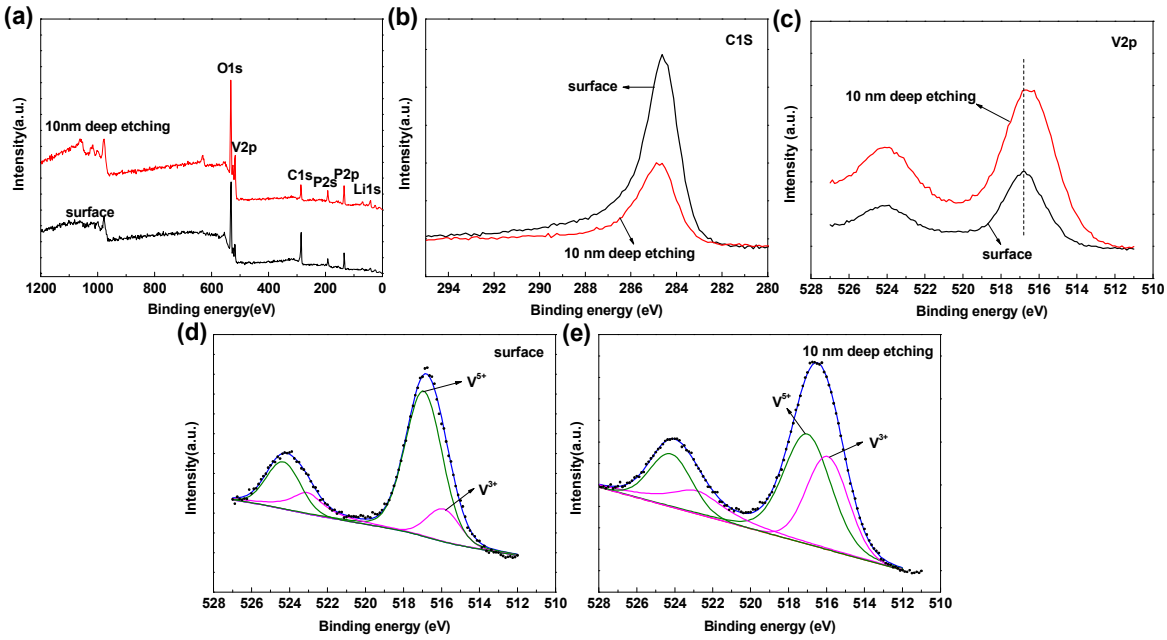

Fig.3 (a) XPS spectra of the as-prepared LVP/C-B, (b) XPS core level of C1s, (c-e) XPS core level of V2p.

Fig. 4 shows the SEM images of the as-prepared LVP/C-A and LVP/C-B. The morphologies of LVP/C-A and LVP/C-B have a significant difference. It can be clearly observed that LVP/C-A presents a flake-like morphology, as reported in our previous work.[16] LVP/C-B that uses the mixed solvent has open macroporous network morphology. The macroporous network morphology is more sufficiently and effectively for electrolyte to permeate into the interior of the electrode when compared with the flake-like morphology, which is beneficial to the electrochemical performance of the cathode material.[22] Although only a small amount of 1, 2-propylene glycol was added to the rheological phase method, such a big change was happened to the morphology of $Li_3V_2(PO_4)_3$/C. This could be ascribed to the large amount of heat produced during the ball grinding process, part of 1, 2-propylene glycol can react to stearic acid and generate propylene glycol monostearate, which may promote the formation of macroporous structure. In order to further investigate the porous structure, N_2 adsorption/desorption isotherms are measured (Fig. 5). The Brunauer–Emmett–Teller (BET) specific surface area of LVP/C-A and LVP/C-B is 23.41 and 30.44 $m^2 g^{-1}$, respectively. The pore size distribution curve indicates that LVP/C-B has mesopores centered at 19 and 37 nm with a total pore volume is 0.07648 ml g^{-1}. However, LVP/C-A only has mesopores centered at 19 nm and the total pore volume is 0.04075 ml g^{-1}. The big specific surface area and porous structure of LVP/C-B can increase the reaction area and speed up the lithium ion transport during the charge/discharge process. The Schematic illustration of the growth mechanism involved in the rheological phase method of $Li_3V_2(PO_4)_3$/C is shown in Fig.6.

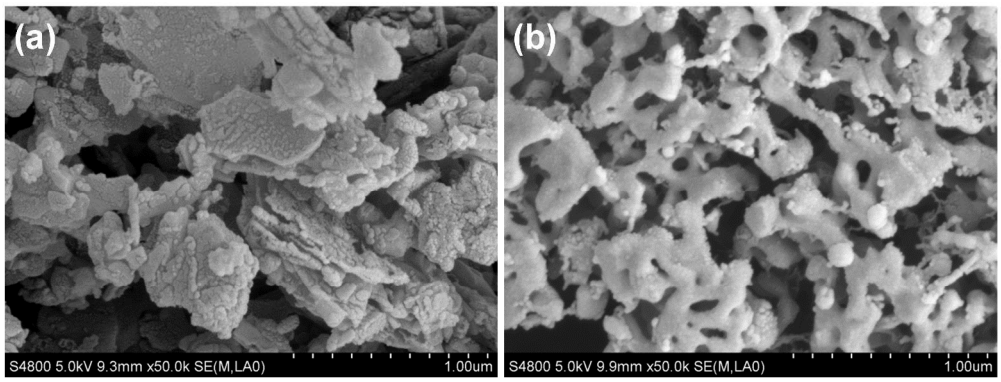

Fig.4 SEM images of the as-prepared $Li_3V_2(PO_4)_3$/C. (a) LVP/C-A and (b) LVP/C-B.

Journal Name RSCPublishing

ARTICLE

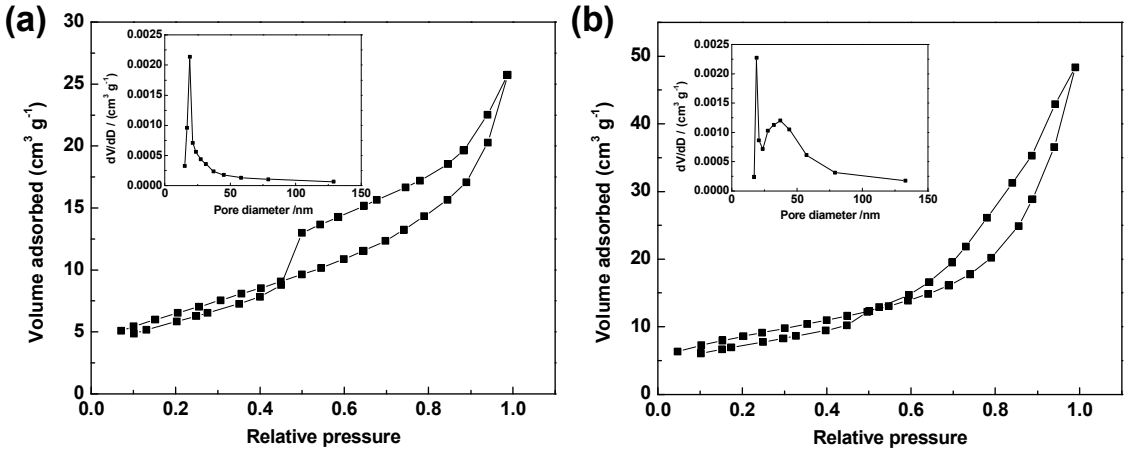

Fig. 5 N_2 adsorption/desorption isotherms and the pore-size distributions (inset) of the LVP/C samples. (a) LVP/C-A and (b) LVP/C-B.

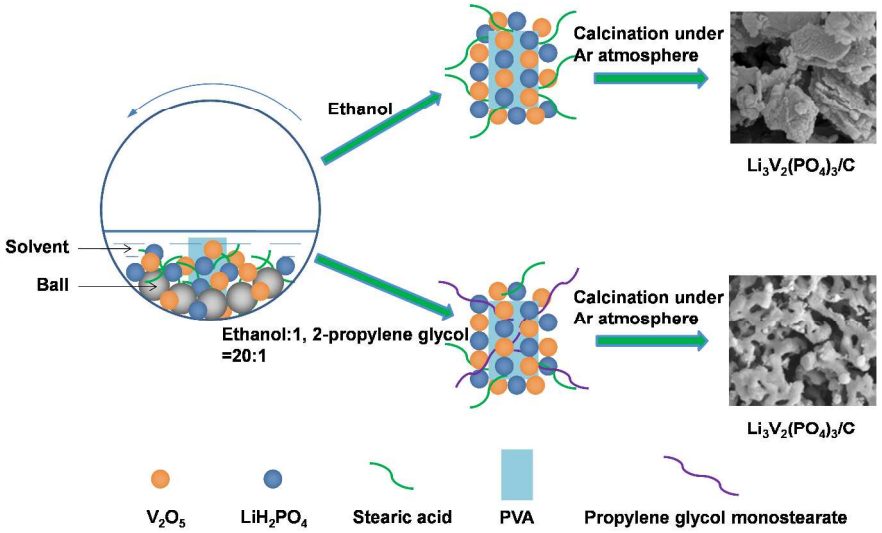

Fig.6 Schematic illustration of the growth mechanism involved in the rheological phase method of $Li_3V_2(PO_4)_3$/C.

Fig. 7(a) shows the initial charge/discharge curves of LVP/C-A and LVP/C-B at 1C in the voltage range of 3.0-4.8V. It is obvious to see four charge plateaus on both of the charge curves, indicating that three lithium ions can be extracted with a theoretical specific capacity of 197 mAh g^{-1}. The mass loading of the LVP/C-A and LVP/C-B are 2.35 mg and 2.24 mg. The initial charge/discharge capacities of LVP/C-A are 161 and 144 mAh g^{-1}, with a coulomb efficiency of 89.4%. LVP/C-B displays higher charge/discharge capacities of 165 and 154 mAh g^{-1}, the coulomb efficiency is as high as 93.3%. Obviously, the preparation of porous morphology can improve the performance of LVP/C.

Journal Name

RSCPublishing

ARTICLE

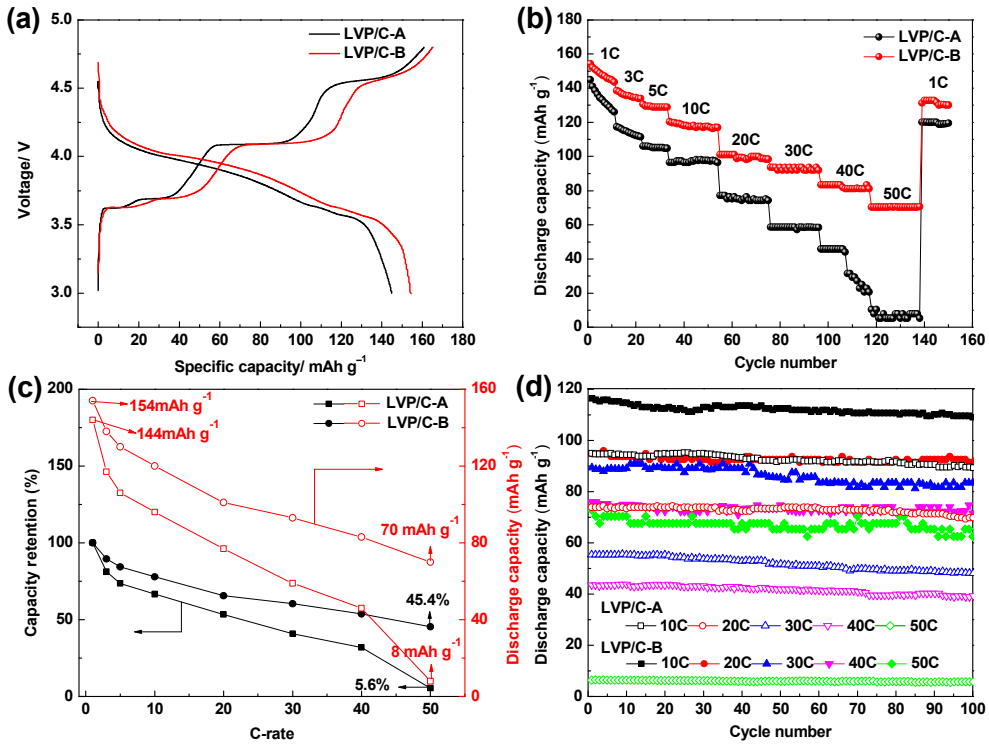

Fig. 7 (a) Initial charge/discharge curve of LVP/C-A and LVP/C-B at 1C between 3.0 and 4.8 V. (b) Rate capabilities of LVP/C-A and LVP/C-B. (c) Capacity retentions of LVP/C-A and LVP/C-B. (d) Cycling performance of LVP/C-A and LVP/C-B at the rate from 10 to 50 C between 3.0 and 4.8 V.

Fig.7(b) shows the rate capabilities for LVP/C-A and LVP/C-B at different rates in the voltage range of 3.0-4.8 V. The LVP/C-B that uses the mixed solvent exhibits a discharge capacity of 154, 138, 130, 120, 101, 93, 83 and 70 mAh g^{-1} at 1 C, 3 C, 5 C, 10 C, 20 C, 30 C, 40 C and 50 C, respectively, which presents a better high rate performance at high voltage when compared with the other reports.[23,24] However, lower discharge capacities of 144, 117, 106, 96, 77, 59, 46 and 8 mAh g^{-1}can be obtained for LVP/C-A at the corresponding rate. When the current density decreases to 1 C after high-rate cycling, the discharge capacities of LVP/C-A and LVP/C-B are 120 and 131 mAh g^{-1}, respectively, which are 83.3% and 85.1% of the initial 1 C. The excellent rate capability of LVP/C-B mainly attributes to the macroporous network morphology. Fig. 7(c) shows the capacity retentions of the two samples. LVP/C-B displays higher capacity retention than LVP/C-A, which maintains 77.9% and 45.4% of the initial specific capacity of 1C at 10 C and 50 C, respectively. However, those of LVP/C-A are only 66.7% and 5.6%. The rate capability of LVP/C-B is much better than LVP/C-A, which indicating that the macroporous network morphology facilitates lithium ion transport.

In order to further study the electrochemical performance of the two samples, the cycling performances of LVP/C-A and LVP/C-B at the rate from 10 to 50 C between 3.0 and 4.8 V after the rate capability test is shown in Fig. 7(d). It can be clear seen that the re-cycling discharge capacities are approximately of the initial discharge capacities of the corresponding rate, demonstrating that the LVP/C composites have excellent reversibility. The LVP/C-B electrode presents good cycling stabilities, with capacity retentions of 93.6%, 97.6%, 93.3%, 93.9% and 88.6% at 10 C, 20 C, 30 C, 40 C and 50 C after 100 cycles, respectively. However, the capacity retentions of LVP/C-A are 94.0%, 94.5%, 86.8%, 90.0% and 88.1% at the corresponding C-rate. Obviously, the cyclic stability of LVP/C-B is improved by the macroporous network morphology.

Fig. 8 shows the Nyquist plots of LVP/C-A and LVP/C-B, which is used for discussing the electrochemical kinetic properties. On the basis of Barsoukov's view,[25] an intercept of the Z' axis in the ultra-high frequency region accords with the ohmic resistance (R_e), combining with the resistance of lithium ions and electrons getting through the electrolyte. The semicircle in the high frequency region is resistance that lithium ions get through the insulating layer of active material (R_{sl}), namely the resistance of solid electrolyte interface (SEI). The semicircle in the middle frequency region represents charge transfer resistance (R_{ct}), the so-called electrochemical reaction resistance is in this zone as well. The sloping line in the low frequency region indicates the Warburg resistance (W), which is related to the diffusion of lithium ion in material particle. The fitting impedance parameters according to the equivalent circuit are presented in Table 1, it can be clearly seen that LVP/C-B exhibits smaller R_{sl} and R_{ct} which means that the 3D network structure of $Li_3V_2(PO_4)_3$/C by using mixed solvent would

effectively enhance the charge-transfer process at the interface between the $Li_3V_2(PO_4)_3$ particles and the electrolyte solution. It may be the main reason that LVP/C-B has higher rate capability than LVP/C-A.

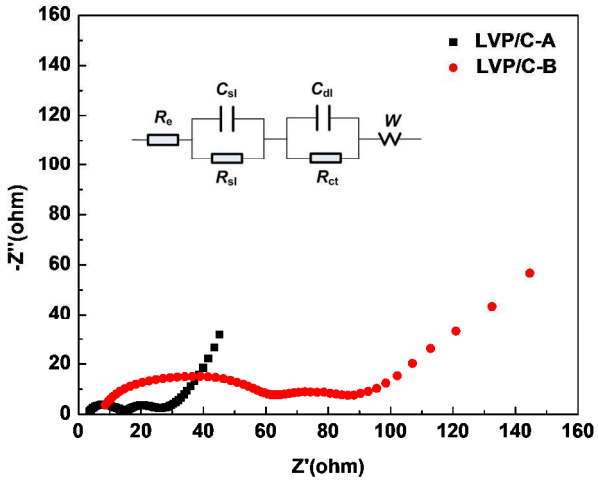

Fig. 8 Electrochemical impedance spectra (EIS) of LVP/C-A and LVP/C-B

Table 1 Evaluated impedance parameters according to the equivalent circuit of the samples

Samples	R_e (Ω)	R_{sl} (Ω)	R_{ct} (Ω)
LVP/C-A	5.605	52.87	26.65
LVP/C-B	2.925	10.8	13.88

4. Conclusions

In this study, we reported an open macroporous network $Li_3V_2(PO_4)_3$/C (LVP/C-B) cathode material obtained via rheological phase method using ethanol and 1,2-propylene glycol as a mixed solvent. It is demonstrated that LVP/C-B achieves a more outstanding rate capability than flake-like LVP/C-A that prepared by single ethanol solvent, which delivers discharge capacities of 154, 130, 93 and 70 mAh g^{-1} at 1 C, 5 C, 30 C and 50 C rates in the voltage range of 3.0-4.8 V, respectively. The EIS results indicate that LVP/C-B has lower charge transfer resistance than LVP/C-A. The exciting results may be related to the macroporous network morphology, which can sufficiently and effectively for electrolyte to permeate into the interior of the $Li_3V_2(PO_4)_3$/C electrode and benefit for the transformation of electrons and lithium-ions.

Acknowledgements

This work was supported by the China Postdoctoral Science Foundation (No. 2014M562322) and Research Fund for the Doctoral Program of Higher Education, the Ministry of Education (No. 20120181120103).

Notes and references

[a]School of Chemical Engineering, Sichuan University, Chengdu, 610065, China. E-mail:tangfedora@163.com
[b]Polymer Research Institute, Sichuan University, Chengdu, 610065, China

1. F. Teng, Z. H. Hu, X. H. Ma, L. C. Zhang, C. X. Ding, Y. Yu and C. H. Chen, *Electrochim. Acta*, 2013, **91**, 43.
2. W. F. Mao, J. Yan, H. Xie, Z. Y. Tang and Q. Xu , *J. Power Sources*, 2013, **237**, 167.
3. J. Gaubicher, C. Wurm, G. Goward, C.Masquelier and L. Nazar, *Chem. Mater.*, 2000, **12**, 3240.
4. C. Wang, H. M. Liu and W. S. Yang, *J. Mater. Chem.*, 2012, **22**, 5281.
5. Q. J. Liu, F.Yang, S. P.Wang, L. J. Feng, W. J. Zhang and H. Y. Wei, *Electrochim. Acta*, 2013, **111**, 903.
6. Z. Y. Chen, H. Z. Jin, C. S. Dai, G. Wu, M. Nelson and Y. F. Cheng, *Int. J. Electrochem. Sci.*, 2013, **8**, 8153.
7. J. Zhai, M. S. Zhao, D. D. Wang and Y. Q. Qiao, *J. Alloys Compd.*, 2010, **502**, 401.
8. R. Y. Zhang, Y. Q. Zhang, K. Zhu, F. Du, Q. Fu, X. Yang, Y. H. Wang, X. F. Bie, G. Chen and Y. J.Wei, *ACS Appl. Mater. Inter.*, 2014, **6**, 12523.
9. L. L. Zhang, G. Liang, G. Peng, F. Zou, Y. H. Huang, M. C. Croft and A. Ignatov, *J. Phys. Chem. C*, 2012, **116**, 12401.
10. Y. Xia, W. K. Zhang, H. Huang, Y. P. Gan, C. G. Liand X. Y. Tao, *Mter. Sci. Eng. B*, 2011, **176**, 633.
11. H. P. Liu, S. F. Bi, G. W. Wen, X. G. Teng, P. Gao, Z. J. Ni, Y. M. Zhu and F. Zhang, *J. Alloys Compd.* 2012, **543**, 99.
12. A. Q. Pan, J. Liu, J. G. Zhang, W. Xu, G. Z. Cao, Z. M. Nie, B. W.Arey and S. Q. Liang, *Electrochem. Commun.*, 2010, **12**, 1674.
13. W. C. Duan, Z. Hu, K. Zhang, F. Y. Cheng, Z. L. Tao and J. Chen, *Nanoscale*, 2013, **5**, 6485.
14. W. F. Mao, C. X. Ma, Y. Ma and Z. Y. Tang, *Ionics*, 2014, **20**, 897.
15. C. L. Wei, W. He, X. D. Zhang, F. X. Xu, Q. Z. Liu, C. Y. Sun and X. Song, *Rsc Adv.*, 2015, **5**, 54225.
16. Y. Y. Wang, Y. Tang, B. H. Zhong, H. Liu, Y. J. Zhong and X. D. Guo, *J. Solid State Electr.*, 2014, **18**, 215.
17. Q. Z. Ou, Y. Tang, Y. J. Zhong, X. D. Guo, B. H. Zhong, L. Hengand M. Z. Chen. *Electrochim. Acta*, 2014, **137**, 489.
18 Y. Tang, Q. Z. Ou, Y. J. Zhong, H. Liu, B. H. Zhong, X. D. Guo and M. Z. Chen, *Mater. Lett.*, 2015, **142**, 189.
19. C. X. Huang, D. D. Chen, Y. Y. Huang and Y. L. Guo, *Electrochim. Acta*, 2013, **100**, 1.
20. W. J. Hao, H. H. Zhan and J.Yu, *Mater. Lett.*, 2012, **83**, 121.
21. Y. Tang, B. H. Zhong, X. D. Guo, H. Liu, Y. J. Zhong, X. Nie and H. Tang, *Acta Phys. Chim. Sin.*, 2011, **27**, 869.
22. L. Zhang, H. F. Xiang, Z. Li and H. H.Wang, *J. Power Sources*, 2012, **203**, 121.
23. L. L. Zhang, S. Duan, G. Peng, G. Liang, F Zou and Y. H. Huang, *J. Alloys Compd.*, 2013, **570**, 61.
24. L. L. Zhang, G. Peng, G. Liang, P. C. Zhang, Z. H. Wang, Y. Jiang, Y. H. Huang and H. Lin. *Electrochim. Acta*, 2013, **90**, 433.
25. Q. C. Zhuang., S. D. Xu, X. Y. Qiu, Y. L. Cui, L. Fang and S. G. Sun, *Process Chem.*, 2010, **22**, 1044.